Numerical Investigation of Shock Waves as Detonation Initiator

S. Bengoechea, J. Reiss, M. Lemke, J. Sesterhenn
Institut für Strömungsmechanik und Technische Akustik (ISTA),
Technische Universität Berlin, Germany

1 Introduction

Pulse detonation engines (PDEs) are quasi-isochoric and offer an efficiency gain compared with well-established constant-pressure combustors [1]. However, the direct initiation of detonations requires a substantial amount of energy in a short time, so that an indirect initiation via deflagration-to-detonation transition (DDT) is desired. One realization is via deflagration-induced shock waves. These ignite the detonation at the focal point, as was demonstrated by [2, 3].

The present study numerically investigates in detail the detonation initiation at the focal point of the imploding shock wave. The combustion chamber under consideration is a circular pipe with one convergent-divergent axisymmetric obstacle [3]. The nozzle-shaped geometry, sketched in Figure 1, has a blockage ratio (BR) of 75 %, a converging angle of 45° and a diverging angle of 131°. The results describe the aspects of the onset of detonation via focusing shock waves.

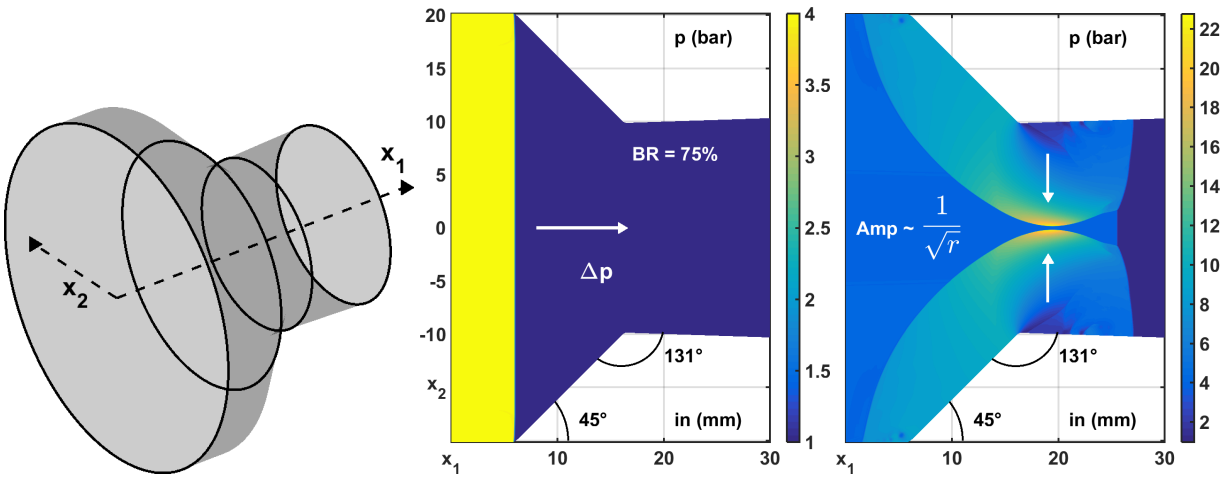

Figure 1: Axial-symmetric shock-focusing nozzle (left), start condition (center) and imploding shock wave after reflection (right).

2 Numerical Methods

The compressible reactive Navier-Stokes equations (1) are solved numerically. These are given in skew-symmetric form with the computational variables set to $[\sqrt{\rho},\ \sqrt{\rho}u_i,\ p,\ \rho Y]^T$. t represents the temporal

Correspondence to: bengoech@tnt.tu-berlin.de

variable, ρ the density, u_i (or u_j, u_k) the i-th (or j-th, k-th) velocity component, p the pressure, τ_{ij} the viscous stress tensor, T the temperature, and δ_{ij} the Kronecker symbol. The case under study allows to write the equations in axial-symmetric form, reducing the domain by one dimension. Hence, the summation convention applies with i, j, $k = 1, 2$.

The axial-symmetric geometry in Figure 1 is mapped onto an equidistant computational space ξ_i. The pole is not discretized, in order to avoid the geometrical singularity $\lim_{x_2 \to 0} 1/x_2$ in the x_2 (radial) direction. The i-th (or j-th, k-th) physical coordinate is denoted by x_i (or x_j, x_k). The divergence and the gradient on an arbitrarily distorted grid can be expressed as $\frac{\partial u_i}{\partial x_i} = \nabla \cdot u = \frac{1}{J} \frac{\partial m_{ji} u_j}{\partial \xi_i}$ and $\nabla p = \frac{1}{J} \frac{\partial m_{ji} p}{\partial \xi_i}$, respectively (see Appendix A).

A good and computationally inexpensive description of the thermodynamics is needed for a faithful representation of the reaction. To this end, the sensible energy is defined as $e_s = \frac{p}{\rho(\gamma(T)-1)} - \frac{p_0}{\rho_0(\gamma(T_0)-1)} = \frac{p}{\rho(\gamma(T)-1)} + const$ [4], with the adiabatic exponent γ temperature dependent. $\gamma(T)$ is constructed with a 7-th order polynomial that closely matches the sensible energy given by the CHEMKIN database [5]. Figure 2 depicts the used γ function and the corresponding sensible energy. Furthermore, this Figure shows that the constant γ approach only applies for a small changes in T. The maximum absolute and relative error made by the polynomial interpolation conforms to $9.6\,K$ and $0.67\,\%$, respectively (see Figure 7 in Appendix B).

$$\sqrt{\rho} \frac{\partial \sqrt{\rho}}{\partial t} + \frac{1}{2} \frac{\partial \rho u_i}{\partial x_i} = 0 \tag{1a}$$

$$\sqrt{\rho} \frac{\partial \sqrt{\rho} u_i}{\partial t} + \frac{1}{2} \left(\frac{\partial \rho u_j u_i}{\partial x_j} + \rho u_j \frac{\partial u_i}{\partial x_j} \right) + \frac{\partial p}{\partial x_i} = \frac{\partial \tau_{ij}}{\partial x_j}, \tau_{ij} = \mu \left(\left(\frac{\partial u_i}{\partial x_j} + \frac{\partial u_j}{\partial x_i} \right) - \delta_{ij} \frac{\partial u_k}{\partial x_k} \right) \tag{1b}$$

$$\frac{\partial}{\partial t} \left(\frac{p}{\gamma - 1} \right) + \frac{\partial}{\partial x_i} \left(\frac{\gamma}{\gamma - 1} u_i p \right) - u_i \frac{\partial p}{\partial x_i} = \frac{\partial u_i \tau_{ij}}{\partial x_j} - u_j \frac{\partial \tau_{ji}}{\partial x_i} - \frac{\partial}{\partial x_i} \left(\lambda \frac{\partial T}{\partial x_i} \right) + \dot{\omega}_T \tag{1c}$$

$$\frac{\partial \rho Y}{\partial t} + \frac{\partial \rho u_i Y}{\partial x_i} = \frac{\partial}{\partial x_i} \left(\rho D \frac{\partial Y}{\partial x_i} \right) + \dot{\omega} \tag{1d}$$

The temporal term $\frac{\partial}{\partial t} \left(\frac{p}{\gamma(T)-1} \right)$ in (1c) requires the implicit solution to extract the thermodynamic quantities (T or p) of the flow for every time step. By assuming that $\frac{\partial}{\partial t} \left(\frac{1}{\gamma(T)-1} \right) \approx 0$ between two consecutive time steps, an explicit relation between the sensible energy and T is given and the numerical effort simplifies considerably. Then this term can be rewritten as $\frac{\partial}{\partial t} \left(\frac{p}{\gamma(T)-1} \right) \approx \frac{1}{\gamma(T)-1} \frac{\partial p}{\partial t}$. The validity of this assumption is checked on-the-fly, see Figure 7 in Appendix B for the results.

The dynamic (shear) viscosity μ is calculated with the Sutherland law, while the mass diffusion coefficient D is described by Fick's law [6]. These determine λ the thermal conduction coefficient.

The gas mixture is stoichiometric hydrogen-air enriched to 40% oxygen ($4H_2 + 2O_2 + 3N_2$). The reaction is modelled by a one global species Y, changing from one (unburned) to zero (burned) and a one-step irreversible reaction. The consumption of Y during the reaction is taken into account by the mass reaction rate $\dot{\omega} = -K_f \rho Y$ and the heat release due to combustion $\dot{\omega}_T = -Q\dot{\omega}$. Q is the heat release per unit mass of fuel [6]. The reaction rate constant is modelled by the Arrhenius law $K_f = Ae^{-\frac{T_a}{T}}$, with the activation temperature T_a and the pressure and temperature dependent pre-exponential factor A. The parameter A is then adjusted to match the induction time of the detailed San Diego kinetics mechanism $\tau_{c_{ref}}$ for the temperature and pressure intervals appearing at the focusing of the shock wave (1200 to 2100 K and 100 to 200 bar).

The good performance of the optimized one-step model in τ_c is evident from the results of the right plot of Figure 2. The maximum relative error in τ_c for the one-step model is $0.033\,\%$.

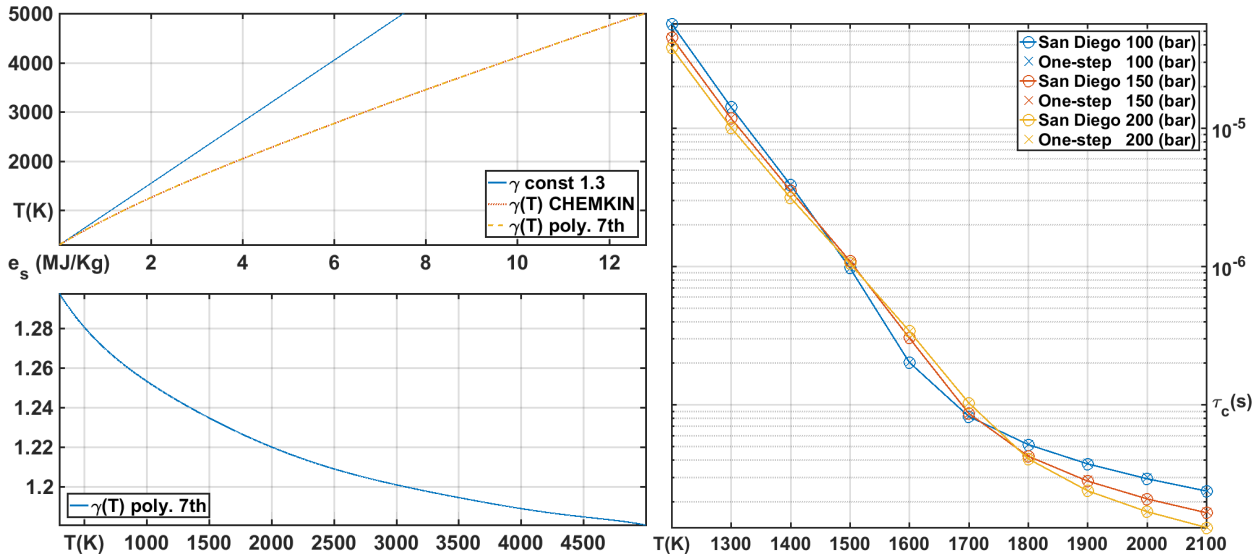

Figure 2: Sensible energy as a function of T (upper left), γ as a function of T (lower left) and induction time τ_c (isochoric) for $4H_2 + 2O_2 + 3N_2$ (right).

Equations (1) are solved with an in-house code, fully MPI parallelized by a layer decomposition approach [3]. 4-th order finite differences central stencils are used to avoid artificial dissipation. The time is also integrated by a 4-th order explicit Runge-Kutta method. The grid consists of $n_1, n_2 = 1024, 2048 \approx 2.1$ millions, computed on 32 CPUs. The west-east boundaries are selected to non-reflecting, while the north-south are set to non-slip adiabatic walls. The reflections at the nozzle of incoming shock waves of Mach numbers $M \approx 1.8, 1.9, 2.0, 2.1, 2.2, 2.3$ with pressure jumps of $\Delta p = 3.5, 4.0, 4.5, 5.0, 5.5, 6.0\,bar$ are analysed. The temperature, pressure and species of the initial premixed gas are specified to $298.15\,K$, $1.01330\,bar$ and 1, respectively. Figure 1 gives an overview of the configuration under study.

3 Results

The reflection of the incoming shock wave at the nozzle creates an imploding (or converging) shock wave (right plot in Figure 1). This type of shock wave forces the shocked gas into an ever-decreasing area, resulting in an additional adiabatic compression that generates high-pressure and high-temperature focal regions [7].

The results for $\Delta p = 6.0\,bar$ depicted in Figure 3 show the direct (or strong) detonation initiation at the focal point. The pre-detonation energy concentration (p and T approx. $350\,bar$ and $2000\,K$) is enough to trigger the detonation. On the other hand, the energy concentration for $\Delta p = 3.5\,bar$ (p and T approx. $95\,bar$ and $1000\,K$) does not suffice to initiate the detonation (results for $\Delta p = 3.5\,bar$ not shown).

Between the no-detonation outcome ($3.5\,bar$) and the strong initiation ($6.0\,bar$) exists an intermediate stage, where the onset of detonation does not coincide with the initial focusing of the imploding shock wave. In the results for $\Delta p = 4.0, 4.5, 5.0, 5.5\,bar$, there is no direct initiation. To illustrate this mild initiation

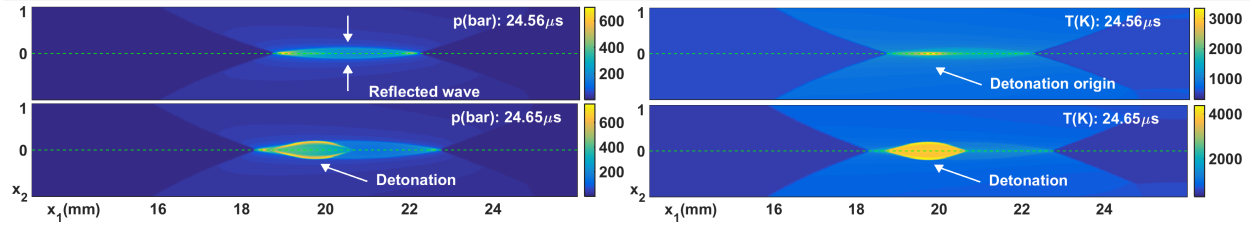

Figure 3: p (left column) and T (right column) evolution of the initiation process for $\Delta p = 6.0\,bar$.

mechanims, the next analysis is concentrated in the incoming shock wave of $\Delta p = 4.0\,bar$. The findings also apply to the incoming shock wave strengths of $\Delta p = 4.5, 5.0, 5.5\,bar$.

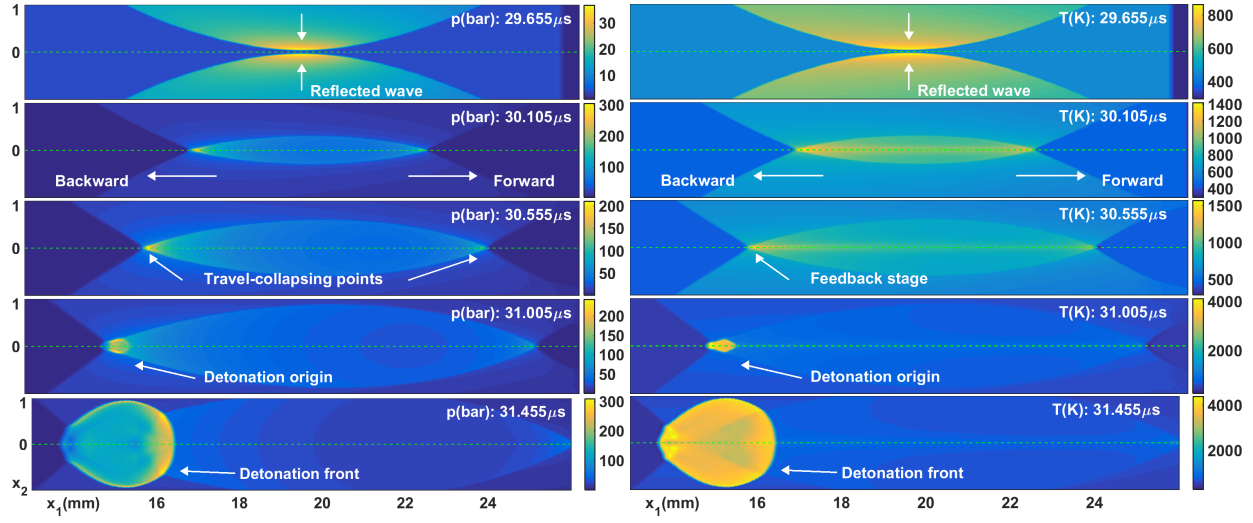

Figure 4: p (left column) and T (right column) evolution of the initiation process for $\Delta p = 4.0\,bar$.

The spatial curvature of the converging shock wave favours the consecutive sequence of focusing events along the center line. This develops two collapsing points travelling backwards and forwards, i.e. travel-collapsing points (see Figure 4).

The initial focusing stage ignites the reaction, as Figure 5 shows in the consumption of Y. Subsequent to the initial focusing, the pressure decays for both travel-collapsing points, marked with A (Backward) and C (Forward) in Figure 5. The backwards point presents a steady increase in temperature supported by the heat released due to combustion (marked with B). This temperature increment further accelerates the reaction rate of the mixture and a higher amount of heat is released, what amplifies the temperature amplitude of the backwards point, establishing a positive feedback. Consequently, the detonation arises from the backwards point, which is restructured into a coupled combustion-pressure wave (marked with D in Figure 5). The feedback stage is enabled by the curvature of the imploding shock. The continuous deceleration of the focusing events gives the reaction enough time to develop and allows for a feedback with the travel-collapsing point.

The results for the forwards travel-collapsing point (marked with C in Figure 5) do not show a successful detonation initiation. The lower deceleration suffered by this travel-collapsing point prevents the coherence

in time between this point and the progressing reaction. The resulting temperature following the initial focusing is not substantially lower than the backwards point and likely plays a minor role in the non-successful initiation.

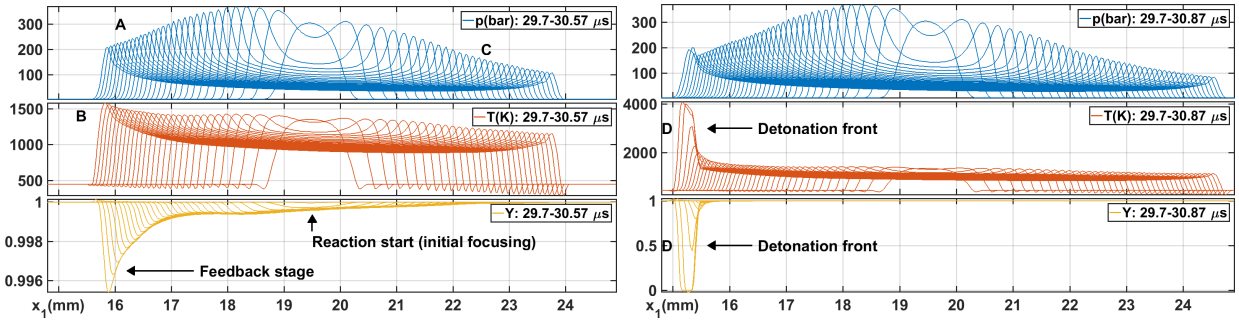

Figure 5: p, T and Y from the center line superimposed in time for $\Delta p = 4.0\,bar$. Initial focusing and feedback (left column), detonation onset (right column). Legend indicates the time interval.

The velocities of the travel-collapsing points (V_{tc}) and the reaction fronts (V_{rf}) are visualized in Figure 6. The firstly infinite value of V_{tc} (due to the flat peak of the imploding shock) suffers a strong deceleration as the curvature increases in the simulation results of $\Delta p = 4.0, 4.5, 5.0, 5.5\,bar$. Both fronts (collapsing point and reaction) coincide during the feedback stage but solely the backwards point undergoes to detonation. This points present in the results an abrupt transition prior to converging to CJ velocity.

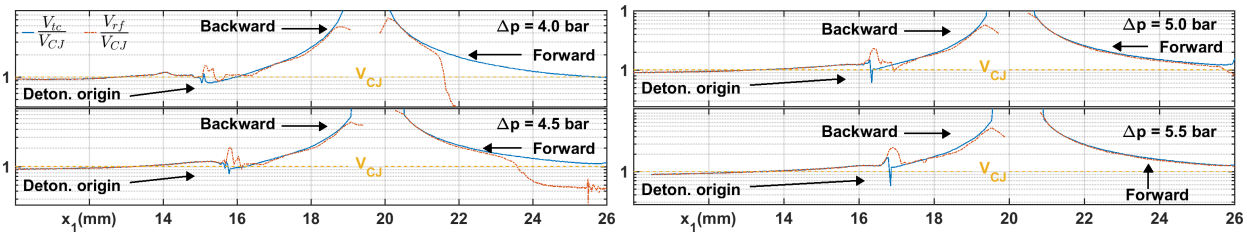

Figure 6: Velocities of the travel-collapsing points (V_{tc}/V_{CJ}) and the reaction fronts (V_{rf}/V_{CJ}).

4 Conclusions

The details in the onset of detonation via focusing shock waves are revealed. From the results, the initiation process is classified as mild or strong, depending on the incoming shock wave pressure (Δp). The values of pressure and temperature at the focal area dominate the process in strong initiations ($\Delta p = 6.0\,bar$). For weaker incoming shocks ($\Delta p = 4.0, 4.5, 5.0, 5.5\,bar$), the deceleration of the sequential focusing events along the center line is decisive for a successful mild initiation.

Acknowledgements The authors gratefully acknowledge support by the Deutsche Forschungsgemeinschaft *DFG* as part of the collaborative research center *SFB-1029* "Substantial efficiency increase in gas turbines through direct use of coupled unsteady combustion and flow dynamics".

Appendix A. Axial-symmetric geometry factors for arbitrarily distorted Grids

$$\frac{\partial u_i}{\partial x_i} = \nabla \cdot u = \frac{1}{J}\frac{\partial m_{ji} u_j}{\partial \xi_i} = \frac{1}{J}\left(\frac{\partial}{\partial \xi_1}(m_{11}u_1 + m_{21}u_2) + \frac{\partial}{\partial \xi_2}(m_{12}u_1 + m_{22}u_2)\right)$$

$$\nabla p = \frac{1}{J}\frac{\partial m_{ji} p}{\partial \xi_i} = \begin{pmatrix} \frac{1}{J}\frac{\partial m_{11} p}{\partial \xi_1} & \frac{1}{J}\frac{\partial m_{12} p}{\partial \xi_2} \\ \frac{1}{J}\frac{\partial m_{21} p}{\partial \xi_1} & \frac{1}{J}\frac{\partial m_{22} p}{\partial \xi_2} \end{pmatrix}, m_{ij} = \begin{pmatrix} x_2\frac{\partial x_2}{\partial \xi_2} & -x_2\frac{\partial x_2}{\partial \xi_1} \\ -x_2\frac{\partial x_1}{\partial \xi_2} & x_2\frac{\partial x_1}{\partial \xi_1} \end{pmatrix}, J = x_2\left(\frac{\partial x_1}{\partial \xi_1}\frac{\partial x_2}{\partial \xi_2} - \frac{\partial x_1}{\partial \xi_2}\frac{\partial x_2}{\partial \xi_1}\right)$$

Appendix B. Error estimation in the thermodynamic model

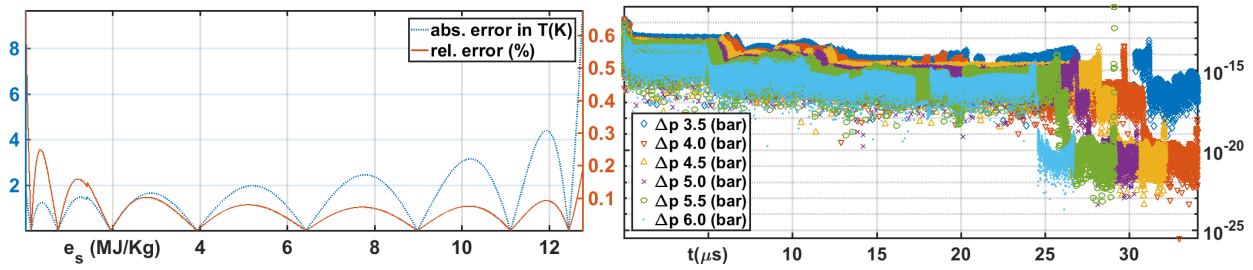

Figure 7: Relative and absolute error in T with 7-th order polynomial interpolation (left). $\frac{\partial}{\partial t}(\frac{1}{\gamma(T)-1}) \approx \frac{1}{dt}(\frac{1}{\gamma(T)-1|_{t^{n+1}}} - \frac{1}{\gamma(T)-1|_{t^n}}) \approx 0$ with a maximum error of $9.5 \cdot 10^{-12}$ (right).

References

[1] Kailasanath K. (2000). Review of propulsion applications of detonation waves. AIAA Journal Vol. 38, No. 9.

[2] Gray JAT, Lemke M, Reiss J, Paschereit CO, Sesterhenn J, Moeck JP. (2017). A compact shock-focusing geometry for detonation initiation: Experiments and adjoint-based variational data assimilation. Combustion and Flame, 183:144-156.

[3] Bengoechea S, Gray JAT, Reiss J, Moeck JP, Paschereit OC, Sesterhenn J. (2018). Detonation initiation in pipes with a single obstacle for mixtures of hydrogen and oxygen-enriched air. Combustion and Flame, 198:290-304.

[4] Lefebvre MH, Oran ES, Kailasanath K. (1992). Computations of detonation structure: The influence of model input parameters. Naval Research Laboratory. Report number NRL/MR/4404-92-6961.

[5] O'Connaire M, Curran HJ, Simmie JM, Pitz WJ, Westbrook CK. (2004). A Comprehensive Modeling Study of Hydrogen Oxidation. International Journal of Chemical Kinetics, 36:603-622.

[6] Poinsot T, Veynante D. (2005). Theoretical and numerical combustion, 3-rd Edition.

[7] Jackson SI, Shepherd JE. (2008). Detonation Initiation in a Tube via Imploding Toroidal Shock Waves. AIAA Journal, Vol. 46, No. 9.